Multiphase measurement of blood flow in a microchannel

Joseph M. SHERWOOD[1, 2*], David HOLMES[3], Efstathios KALIVIOTIS[2], Stavroula BALABANI[2]

* Corresponding author: Tel.: ++44 (0)207 5941850; Email: joseph.sherwood@imperial.ac.uk
1: Department of Bioengineering, Imperial College London, UK
2: Department of Mechanical Engineering, University College London, UK
3: Sphere Fluidics Limited, Babraham Research Campus, Cambridge, UK

Abstract Blood is a complex fluid comprising red blood cells (RBCs) suspended in a continuous medium. Recent studies have shown that the spatial concentration distributions of the RBCs have a considerable impact on their velocity distributions. By extending this analysis, we present the first multiphase experimental analysis of microscale blood flow to include local velocity and concentration distributions of both phases of the blood. Human blood is perfused though a PDMS microchannel comprising a sequentially bifurcating geometry with a 50×50μm cross-section. The flow rate and the proportion of flow entering the branches of the bifurcation are varied, and the effects on the velocity and concentration distributions of the RBCs and suspending medium are analysed. In addition, the influence of RBC aggregation is investigated. The relative velocity between the two phases of the blood is shown to be dependent to varying degrees on all of the independent parameters examined in this study. A mechanism for the observed trends based on collisions of RBCs with the channel walls in the bifurcation is proposed.

Keywords: Micro particle image velocimetry, haematocrit distribution, microcirculation, multiphase.

1. Introduction

Detailed knowledge of blood flow characteristics is of fundamental importance in understanding a wide range of physiological and pathological functions. The multiphase nature of blood, being composed of discrete cells suspended in a continuous medium, drastically alters its flow characteristics from those of a simple fluid such as water. However, these characteristics are often overlooked or considered unimportant in haemodynamic studies. When measured in rheometers, blood displays shear thinning properties; reported to be a result of red blood cell (RBC) aggregation at low shear rates and RBC deformation at high shear rates. Additionally, the viscosity of blood is highly dependent on the haematocrit (RBC concentration) and increases around 4 times as the haematocrit increases from 0 up to 0.45, the latter being physiological haematocrit in the large vessels. It has been widely observed that RBCs migrate away from the wall, forming a region of low RBC concentration commonly termed a cell-depleted layer (CDL), in long straight vessel sections which is enhanced around bifurcations (Ong et al., 2012; Sherwood et al., 2012). It is often considered that the haematocrit is zero in the CDL and constant in the RBC core. However, this is an oversimplification, which has significant ramifications; local viscosity, and hence local velocity, is strongly affected by RBC concentration at a given location. Hence, any conclusions based on the binarisation of the haematocrit distribution with regards to, for example, wall shear stress, may be specious. Instead, we opined that it is more appropriate to consider the RBC concentration as a continuous distribution (Sherwood et al., 2014b). An increasingly common method of measuring blood flow is micro particle image velocimetry (μPIV): a non-invasive method for extracting Eulerian flow field information from images. Poelma et al. (2012) provided much needed details on the effect of using images of RBCs or suspended tracer particles on the underestimation of velocities due to out of plane particles/cells. They concluded that for medium magnification (12.5×) objectives,

both methods underestimate velocity by approximately the same amount, due to 'depth saturation'. However, their analysis made the tacit assumption that the two methods should, in the absence of error, yield the same result. The use of microparticles suspended in the flow to capture a velocity field is based on the condition that the particles are neutrally buoyant and sufficiently small that they follow the flow field without influencing it. As the microparticles are suspended in the continuous suspending medium (SM), the measured flow field will thus represent the velocities of the SM. However, PIV measurements based on images of RBCs would give information on the cell velocity. Given the multiphase nature of blood and the heterogeneous concentration distribution of RBCs (and hence SM) throughout the vasculature, we propose that the RBC and SM velocities are likely to differ significantly. In the present study, a system is developed which allows quasi-simultaneous measurements of both phases of the blood. Information on the spatial haematocrit distribution is extracted from the same images, yielding for the first time (to the authors' knowledge) complete multiphase measurements of blood flow. The system is used to examine human blood flowing through a sequentially bifurcating microchannel under a range of flow conditions.

2. Methods

Details of the experimental setup and methodologies used in the present study have been reported previously (Sherwood et al. 2014b) and are described briefly below. Human blood was collected via venepuncture and mixed with 1.8 mg/ml EDTA to prevent coagulation. The samples were separated via centrifugation and the plasma and buffy coat removed. The RBCs were then washed twice in PBS and resuspended at a haematocrit of 0.25. Neutrally buoyant 1.1 μm fluorescent microparticles (Invitrogen) were added at a volume concentration of 0.1% to provide the velocity of the SM and for certain cases, Dextran 2000 at 5 *mg/ml* was added to induce RBC aggregation. The experimental setup used for the present study is shown in Fig. 1.

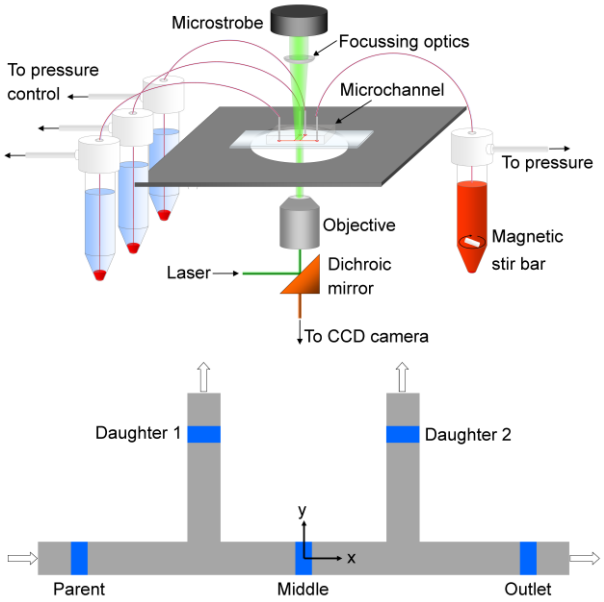

Figure 1: Schematics of the experimental setup and the microchannel. Arrows indicate flow directions. Shaded areas indicated averaging regions for profiles.

The experimental system comprised a polydimethylsiloxane (PDMS) microchannel bonded to a glass microscope slide with sequential 90° bifurcations, with 5 channel widths between them, and a 50×50μm cross-section. The pressure in each branch of the channel was regulated using a Fluigent MFCS system. The microchannel was placed on an inverted microscope with a 10× air objective and illuminated alternately with Nd:YAG laser (New Wave Solo) and microstrobe LED illumination. Images were captured on a CCD camera (Hamamatsu C8484-05CP). All acquisition was carried out using a custom system built in LabVIEW. The strobe and laser illuminated images were processed using ensemble averaged PIV algorithms (http://www.jpiv.vennemann-online.de/) to yield a final vector spacing of 4 pixels equivalent to 2.6μm, with 50% overlap. Vector magnitudes were multiplied by a factor of 1.5, to adjust for the underestimation predicted by Poelma et al. (2012) and invalid vectors were identified using the normalised median test (Westerweel and Scarano, 2005) and replaced with the median of the surrounding vectors.

The strobe images were further processed to yield haematocrit distributions, using a development of the method described in a previous study (Sherwood et al. 2014a). Based

on the cross sectional symmetry of the microchannel, the measured velocity and concentration distributions were extended into three dimensions for flux calculations, as described previously (Sherwood et al. 2014b).
The branches are considered separately by averaging velocities axially in the blue shaded sections indicated in Figure 1. The square sides of the microchannel result in optical distortion near the channel edges, thus the first viable vectors were at x^*=±0.4. For calculation of flow rates/fluxes the data were extrapolated. For the SM, it is reasonable to assume that the no-slip condition is applicable; hence a zero wall velocity is assumed. For the RBCs, the acquired images show that the wall velocity is non-zero: RBCs adjacent to the wall tend to roll along it with a finite velocity. Hence, the wall velocity for the RBCs was estimated by linearly extrapolating the velocity profiles from the three vectors closest to the wall.
The flux of RBCs in a given branch, *i*, as calculated according to

$$\frac{Q_{rbc,i}}{w^2} = \int_{-0.5}^{0.5}\int_{-0.5}^{0.5} U_{rbc}\left(y^*,z^*\right)H\left(y^*,z^*\right)dy\,dz \qquad (1)$$

Where *w* is the channel width, y^* and z^* are the channel coordinates normalised by *w* and *H* is the local haematocrit. For the suspending medium

$$\frac{Q_{sm,i}}{w^2} = \int_{-0.5}^{0.5}\int_{-0.5}^{0.5} U_{sm}\left(y^*,z^*\right)\left(1-H\left(y^*,z^*\right)\right)dy\,dz \qquad (2)$$

The total flux is defined as the sum of the RBC and suspending medium fluxes.
To characterise the difference between the velocities of the two phases, we define a parameter, U_ϕ^* according to

$$U_\phi^* = \frac{\int_{-0.5}^{0.5}\int_{-0.5}^{0.5} U_{rbc}\left(y^*,z^*\right)-U_{sm}\left(y^*,z^*\right)dy\,dz}{Q_{tot}/w^2}\times 100\% \qquad (3)$$

In order to isolate the calculation of U_ϕ^* from the wall velocity assumptions, U_ϕ^* is calculated with limits on the integrals in Equations 1-3 of ±0.4 instead of ±0.5 (with the exception of the insets of Figure 3).
Cumulative uncertainties for all data were calculated using the chain rule of differentiation, and errorbars shown in the figures indicate one standard deviation. Due to the non-linear nature of the reported trends, tests for statistical significance are carried out using the non-parametric Spearman's rank correlation coefficient, ρ and corresponding *p*-value.
Data was acquired for 44 Dextran (aggregating) and 33 PBS (non-aggregating) cases at a range of parent branch flow rates and flow ratios.

3. Results

To illustrate the difference in velocity between the two phases, Figure 2 shows some sample velocity profiles in the parent branch. For the PBS cases, the RBC velocity is greater than the SM velocity for both high (Fig. 2d) and low (Fig. 2b) normalised flow rates ($U^*=Q_{tot}/w^3$ s^{-1} : giving channel widths per second). For the Dextran cases, the difference between the two phases is significantly less than for the PBS case at low flow rate (Fig. 2a), and negligible at high flow rate (Fig. 2c).

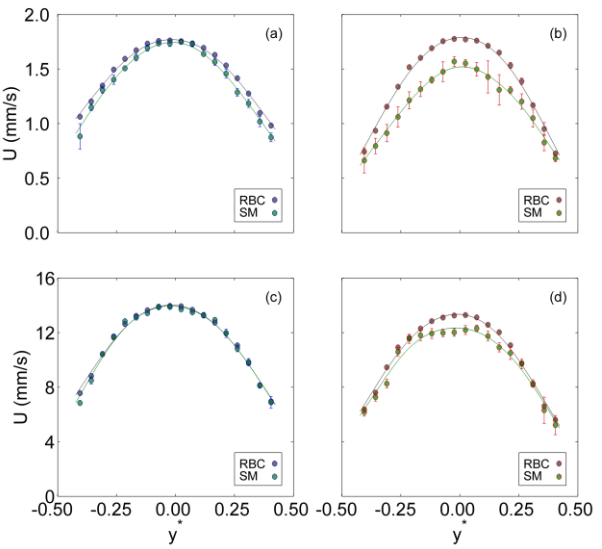

Figure 2: Sample velocity profiles in the parent branch. $y^*=y/w$. Low velocity (a) Dex: U^*=18.7 s^{-1}, (b) PBS: U^*=15 s^{-1}. High velocity (c) Dex: U^*=151.7 s^{-1}, (d) PBS: U^*=130.3 s^{-1}. Curves show spline fits for visualisation purposes.

In order to probe the influence of flow rate on the difference between the velocities, the relative velocity U_ϕ^* is compared to U^* in Figure 3. For the Dextran data (Fig. 3a), there doesn't appear to be a significant trend (ρ=0.068, *p*=0.658), whereas for the PBS data, despite the scatter, a significant trend of

decreasing U_ϕ^* with increasing U^* is observed (ρ=-0.557, p=0.001). This data is calculated only within the central 80% of the channel, as discussed in §2.

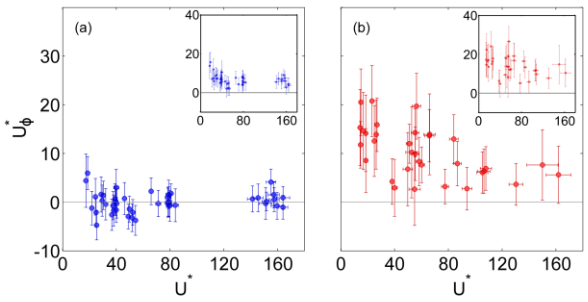

Figure 3: Relative velocity against flow rate in the parent branch (a) Dextran (b) PBS. Insets show the data as calculated including the extrapolation of the velocities at the wall.

However, it is interesting to note that, if the wall extrapolations are taken into account, as shown in the insets, both the Dextran data (ρ=-0.402, p=0.007) and PBS data (ρ=-0.416, p=0.017) show significant trends.

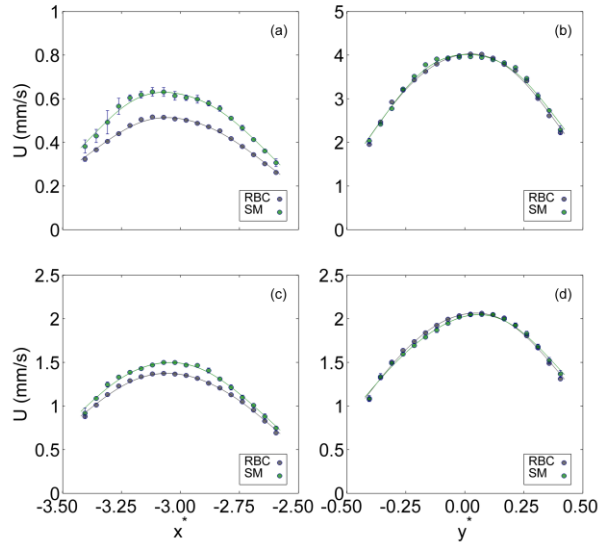

Figure 4: Sample velocity profiles in first bifurcation for Dextran cases. $x^*=x/w$, $y^*=y/w$ Daughter branch 1 (a,c) and middle branch (b,d). (a,b) Low flow ratio: Q_1^*=0.13 (c,d) Q_1^*= 0.42. Curves show spline fits for visualisation purposes.

Figure 4 shows sample velocity profiles for Dextran cases in the first bifurcation at low and high flow ratios, Q^*, defined as the proportion of flow entering a branch from the feed branch. The skewed nature of the velocity profiles is a result of the skewed haematocrit distribution observed in these branches (Sherwood 2014a, 2014b).

The haematocrit and velocity profiles skew in opposite directions, as the local viscosity is increased in regions of elevated haematocrit. At low flow ratio, the difference between the velocities of the RBC and SM is larger in daughter branch 1 (Fig. 4a) than in the middle branch (Fig. 4b), for which the velocities of the two phases are approximately equal. At high flow ratio (Fig. 4c), the difference between the velocities in the daughter branch is less than for low flow ratio, but greater than in the outlet branch (Fig. 4d).

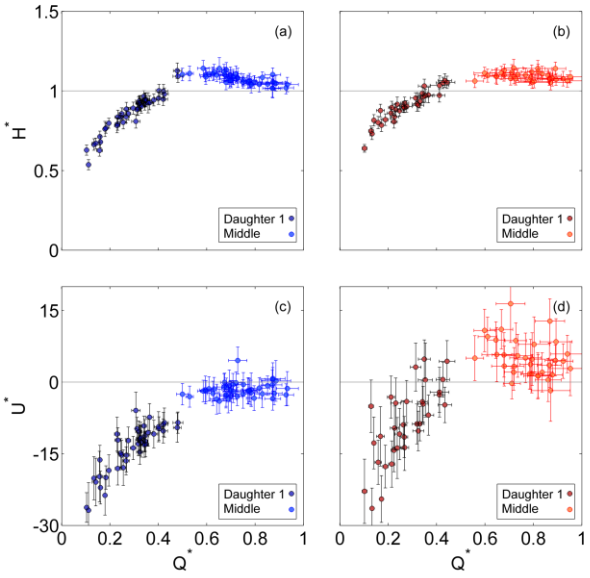

Figure 5: Haematocrit ratio against flow ratio in the first bifurcation (a) Dextran, (b) PBS. Relative velocity against flow ratio in the first bifurcation (c) Dextran, (d) PBS.

While the parent branch haematocrit was constant, the haematocrit in the branching geometry varies due to plasma skimming. It is likely that the RBC concentration and velocity are related to one another, hence the haematocrit ratio, H^* (the branch haematocrit normalised by that in the feed branch for a given case) and the relative velocity are both compared to flow ratio in Figure 5. For both Dextran and PBS data, the haematocrit ratio shows the commonly observed trend for a single bifurcation (Pries et al., 1989), with haematocrit generally reduced for Q^*<0.5, and approaching 1 as the flow ratio increases. For brevity, U_ϕ^* is not graphically compared to H^*, but the statistical trends are reported in the following section.

For both Dextran and PBS data in daughter

branch 1, U_ϕ^* correlates directly with H^* (ρ>0.744, p<0.001), as can be seen by comparing the top and bottom panels in Figure 5. In the middle branch for the Dextran data, U_ϕ^* does not correlate with H^* (p=0.72). Although a correlation between U_ϕ^* and H^* is found for the PBS data (ρ=0.493, p=0.004) in the middle branch, the correlation is not as strong as for daughter branch 1.

In the second daughter branch, the relationships become more complex. As can be seen in Figure 6 (a,b), the haematocrit ratios in the outlet branch and daughter branch 2 are significantly different.

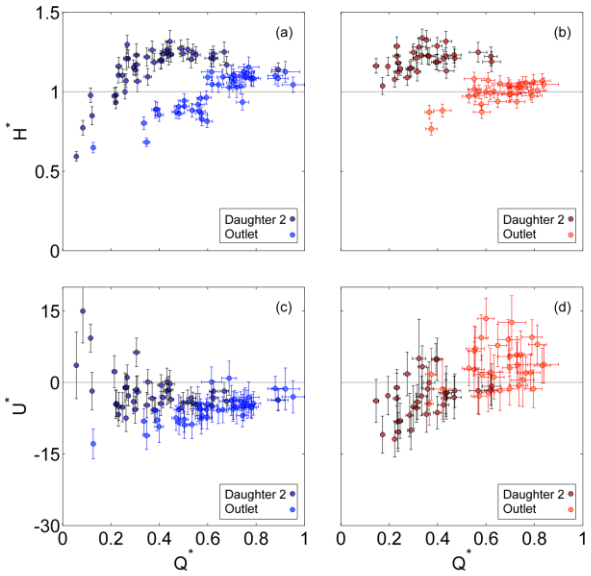

Figure 6: Haematocrit ratio against flow ratio in the second bifurcation (a) Dextran, (b) PBS. Relative velocity against flow ratio in the second bifurcation (c) Dextran, (d) PBS.

The geometry of the bifurcation leads to haematocrit profiles in the middle branch, which are skewed towards the side adjacent to the daughter branches (discussed in detail in Sherwood et al. 2014b, see also Figure 8). As a result, at the second bifurcation, disproportionately more RBCs enter daughter branch 2 than the outlet branch. For the PBS data, the U_ϕ^* vs. Q^* relationship (Fig. 6d), appears to be similar to that observed in the first bifurcation (Fig. 5d). Although H^* correlates with Q^* in both branches (ρ>0.4, p<0.016), U_ϕ^* and H^* are not significantly related (p>0.2). For the Dextran data, H^* correlates with Q^* (Fig. 6 a) in both branches (ρ>0.673, p<0.001). In the outlet branch, there is a strong positive correlation between U_ϕ^* and H^* (ρ=0.787, p<0.001) but no correlation is found in daughter branch 2 (p=0.227).

These seemingly inconsistent trends in U_ϕ^* with Q^* imply that there is another key parameter involved in the relationship. Figure 7 shows the relationship between U_ϕ^* in the bifurcation branches compared to that in the feed branch, $U_{\phi,f}^*$ (parent and middle branches for the first and second bifurcation respectively). For all data except daughter branch 1 for the Dextran samples, there is a strong positive correlation between U_ϕ^* in the feed branch and in the bifurcation (ρ>0.497, p<0.002). For the PBS data in the first bifurcation (Fig. 7b), U_ϕ^* in the middle branch is similar to that in the parent branch, but slightly lower. In daughter branch 1, U_ϕ^* is considerably lower than in the parent branch.

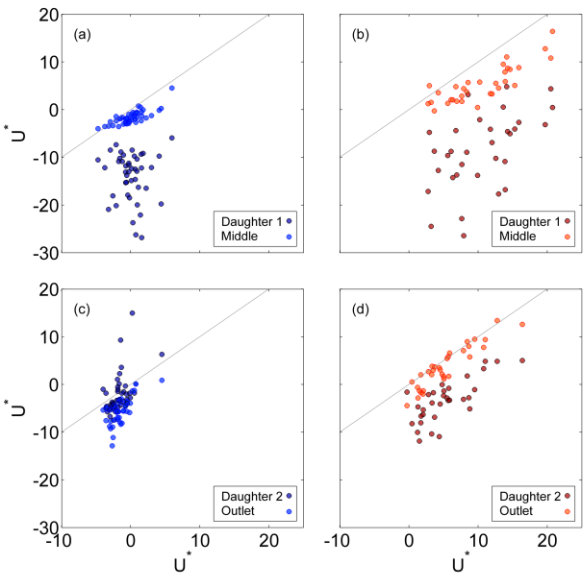

Figure 7: Relative velocity against relative velocity in the feed branch. First bifurcation: feed branch is parent branch (a) Dextran, (b) PBS. Second bifurcation: feed branch is middle branch (c) Dextran, (d) PBS. Grey lines indicate exact match. Error bars have been omitted for clarity, but can be inferred from Figures 3, 5 and 6.

In the second bifurcation, a similar relationship is observed but the differences between the feed branch (middle branch) and the other branches are decreased. For the Dextran data, in the second daughter branch (Fig. 7c), a number of cases in which U_ϕ^* is greater than in the middle branch are observed. By comparison with Figure 6, it is clear that these cases correspond to the low flow ratio cases.

4. Discussion

A number of studies have previously reported on RBC and tracer measurements. Poelma et al. (2012) changed between illumination methods rapidly and repeated measurements *in vivo.* Sugii et al. (2005) carried out combined PTV for tracking RBCs and PIV on fluorescent microparticles. The advanced system of Oishi et al. (2012) enabled simultaneous measurement of the suspending medium and the motion of the RBC membrane at low haematocrit. Both of these *in vitro studies* were carried out in straight channels. The present study adds new insight by reporting simultaneous velocity and concentration measurements and parametrically investigating the influence of aggregation, flow rate, haematocrit and flow ratio.

The data presented in this paper indicates significant differences between the velocities of the RBC and SM. The parameter U_ϕ^*, the average relative velocity as a percentage of the total velocity in the channel, was shown to correlate with a number of parameters examined in the present study. Given the implications of the present data, it seems prudent to start the discussion by considering 'false positive' hypothesis: that the observed differences between the RBC and SM velocities are purely a result of different conditions affecting the PIV processing algorithm.

Depth of correlation

The equation of Olsen and Adrian (2000) used to predict a depth of correlation 37µm for the fluorescent particles. As derivation of this equation is based on idealised Gaussian particle images, it is not directly applicable to RBC image based PIV (we avoid referring to RBCs as tracers for this reason), however based on the brightfield images, it is reasonable to assume that the whole depth of the channel influences the correlation. This would imply that the SM velocities would be underestimated by less than the RBC velocities, and would thus yield negative U_ϕ^* if the true velocities were equal. However, Poelma et al. (2012) reported that contrary to the analytical prediction, for medium magnification (12.5×) objectives, the underestimation of the velocity for a channel of 50µm would be equal for both methods at 0.66, i.e. the measured velocity (at the centreline) would be equal to 0.66 times the actual velocity at the centreline. If the depth of correlation was indeed the case for the observed U_ϕ^*, then positive values would be expected throughout, which is not the case. This does not preclude that the depth of correlation might have some influence, but does imply that it is not the dominant factor.

Haematocrit

Another potential source of difference between the processing of RBC and particle images is the local haematocrit. In order to aid the discussion, Table 1 summarises the significance of the relationships for U_ϕ^* shown in Figures 5, 6 and 7.

Table 1: Summary of significance of observed relationships between U_ϕ^* and other parameters. Blue: Dex, Red: PBS. * < 0.05, ** < 0.01, *** < 0.001.

	Q^*		$U^*_{\phi,f}$		H^*	
Daughter 1	***	***	-	***	***	***
Middle	-	*	***	***	-	**
Daughter 2	-	**	***	***	-	-
Outlet	***	-	***	***	***	-

In daughter branch 1, for both Dextran and PBS data, there is indeed a positive correlation between U_ϕ^* and H^* (see Table 1). However, in the second daughter branch, there was no correlation observed. Additionally, it should be noted that the haematocrit ratio was similar for Dextran and PBS data, and yet the values of U_ϕ^* differed, particularly in the second bifurcation. Furthermore, in the parent branch, the haematocrit was approximately constant (Dextran: 0.158±0.009, PBS: 0.171 ± 0.004: mean±SD), and yet there was a significant trend in the relative velocity with increasing flow rate for the PBS data.

A further difficulty in analysing the influence of the haematocrit is that one would expect the relationship between the RBC and SM velocities to be influenced by local concentrations of RBCs (and hence SM). Thus where trends are observed, it is not possible to state explicitly whether they are observations of a physical phenomenon or the result of an

experimental artefact. Based on the above discussion, while it is plausible that the local haematocrit does influence the PIV processing, the absence of any correlation in half of the branches for both Dextran and PBS cases, suggests that the observed correlation between H^* and $U_\phi{}^*$ are not an experimental artefact.

RBC aggregation

RBC aggregation is a fascinating phenomenon with a wide range of reported effects on blood flow, and yet is commonly dismissed in haemodynamic studies as irrelevant for anything other than low rates. In a previous study (Sherwood et al., 2014a) we observed an influence of aggregation on the shape of the haematocrit and velocity profiles even at high flow rates *in vitro*, in agreement with previous *in vivo* studies (Bishop et al., 2003). In the present study, RBC aggregation clearly influenced the data. In the parent branch, RBC aggregation reduced the relative velocity, (up to 20% in the non-aggregating case) to small values, which are not influenced by flow rate. If the extrapolated wall values are included (inset of Figure 3a), then it seems that aggregation does have an effect at low flow rates, which decreases as the extent of aggregation decreases at higher flow rates. However, the validity of the wall extrapolation is not presently verifiable. Nonetheless, the marked difference between the relative velocity in the Dextran and PBS cases at high flow rates implies that RBC aggregation is still present.

In the first daughter branch, aggregation seems to have a minimal effect, as similar trends in both H^* and $U_\phi{}^*$ are observed (Fig. 5). In the middle branch, the values of $U_\phi{}^*$ correlate very strongly with those in the parent branch (Fig. 7a,b), hence the effect of aggregation is expected to be the same as that in the parent branch. In the second bifurcation, the trends become more complex, as a combination of flow rate and flow ratio combine. Aggregation does not appear to significantly influence H^*, with similar values observed for both aggregating and non-aggregating data (Figs. 5a,b and 6a,b). In the outlet branch, both aggregating and non-aggregating data show strong dependence of $U_\phi{}^*$ on that observed in the middle branch. However, in the second daughter branch, for low flow ratios in the presence of aggregation, the relative velocity was positive, meaning that the RBCs are traveling faster than the suspending medium.

Role of RBC dynamics

Due to the complexity of the data, it would be presumptive to draw solid conclusions regarding the causes behind the observed trends. Rather, this study is intended as an initial investigation into the parameters of interest, and the following *post hoc* analysis provides some possible physical explanations for the observed trends.

RBCs do not aggregate in the PBS cases, and hence each RBC can deform and roll independently, flowing through the suspending medium. For the Dextran case, in which the aggregated RBCs are interconnected, it could be posited that the translation of RBC aggregates draws the local suspending medium along with it, reducing the relative velocity to negligible levels. In the middle and outlet branches, the relative velocity scales very closely with that in the parent branch. Given the geometry (see Figures 1 and 8), it is understandable that the flow is least disrupted by the bifurcations along the straight path (parent, middle, outlet) and hence the relative velocity characteristics observed in one channel section should correspond to the next.

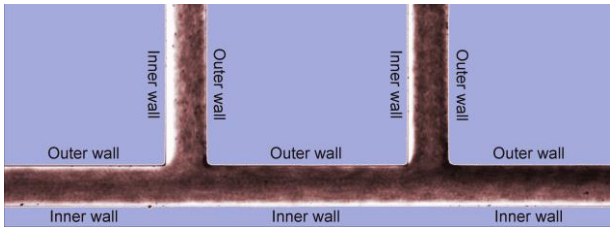

Figure 8: Sample time-average intensity image for Dextran case, U^*=24.5, $Q_1{}^*$= 0.16, $Q_2{}^*$=0.35. Darker sections indicate increased local haematocrit.

Figure 8 shows a sample time-averaged image from a Dextran case, enhanced for clarity. In the first bifurcation (left), the region of highest RBC concentration in the parent branch (in the channel centre) is directed such that there is a region of enhanced RBC concentration at the outer wall of daughter branch 1. This increases

RBC collisions with the wall, which may explain why the velocity of the RBCs is relatively decreased in the daughter branch, giving negative U_ϕ^*. It could be expected that as the haematocrit profile becomes more asymmetric, the relative velocity would decrease as a larger proportion of the RBCs present are close to the wall. As the flow ratio decreases, the distribution of RBCs becomes increasingly skewed (Sherwood 2014b), which is consistent with this theory.

In the middle branch, the haematocrit profiles are also skewed toward the outer wall (see Fig. 8) for similar reasons described above, but by less than in daughter branch 1 (over the flow ratio range considered). If the wall contact is the cause of the reduction in relative velocity, this would decrease U_ϕ^* relative to that in the parent branch. This is indeed what is observed in Figures 7a and b. Continuing this line of reasoning becomes more complex in the second bifurcation, as the haematocrit profile is affected by the flow ratios in both bifurcations and a greater range of sequential flow ratios and flow rates is required to provide further support to this hypothesis.

Limitations

The parameter space that must be covered in order to fully elucidate the interactions between the velocity and concentration of the RBCs and SM is vast, and the present study is limited by only investigating some of the parameter space. A wider range of flow ratios in both branches would be advantageous, as well as more highly resolved flow ratio and flow rate data sets. An additional set of data with a different feed haematocrits would also be advantageous, and would allow for further understanding of the effect of haematocrit. Nonetheless, the use of a sequential bifurcation in the present study allowed more detailed analysis than would have been possible with a single bifurcation.

The absence of absolute flow rates and measured discharge haematocrits in the present study makes it harder to verify the results. However, RBC aggregation imposes experimental time limits of ~ 1 minute before returning the flow rate to a high level to redistribute RBCs evenly throughout the flow system. As a result, syringe pumps are not suitable for the application and the small volumes of blood perfused in a single experimental case are too small to measure.

Measurement of flow rate in the range 0.1-2 μL/min by other means is highly technically challenging without altering the system dynamics. The uncertainties and limitations in the processing methodologies utilised in the present study (PIV and haematocrit distribution estimation) are discussed in depth elsewhere (Sherwood et al. 2014b).

Implications

The data presented in this study has important implications for all research concerning haemodynamics.

In the context of PIV (or PTV) studies, the data implies that it may not be sufficient to use either RBC images or tracer particles in PIV analysis, but rather that both are necessary to completely describe the flow field.

This data adds further support to the assertion that details of the haematocrit distribution are essential in understanding the complex flow fields observed in microscale blood flows, particularly if trying to estimate physiological parameters such as wall shear stress (which is velocity and viscosity dependent).

Although aggregation didn't greatly alter the bulk haematocrit distribution at the bifurcations, its influence on the relationship between the velocities of the two fluid phases was significant. In studies in animals such as rats or chicken embryos, in which RBC aggregation is absent, care should be taken when considering implications for human haemodynamics.

The high resolution of the present data lends itself perfectly as a validation tool for the increasing number of computational models which model individual RBCs within a continuous suspending medium (Fedosov et al., 2011; Freund, 2014). Such models should be able to provide additional insight into the cases of the observed trends.

5. Conclusions

The present study has provided the first report of multiphase experimental measurements of microscale blood flow, taking into account the

velocity and concentration of the RBCs and suspending medium. The data revealed that the relative velocity between the two phases is dependent on the aggregation state, the flow rate, the proportion of flow entering a bifurcation and the 'history' of the haemodynamic environment. Detailed measurements of human blood at physiological haematocrit for small arterioles have shown the highly complex, multiphase nature of blood at this scale. It is hypothesised that the relative velocity is altered by aggregation in parent branch and the collisions of RBCs with the channel wall in the bifurcation. This preliminary study provides the basis for a new approach to analysing microhaemodynamics.

References

Bishop, J.J., Nance, P.R., Popel, A.S., Intaglietta, M., Johnson, P.C., 2003. Relationship between erythrocyte aggregate size and flow rate in skeletal muscle venules. American Journal of Physiology-Heart and Circulatory Physiology 286, H113–H120.

Fedosov, D.A., Pan, W., Caswell, B., Gompper, G., Karniadakis, G.E., 2011. Predicting human blood viscosity in silico. Proceedings of the National Academy of Sciences 108, 11772–11777.

Freund, J.B., 2014. Numerical Simulation of Flowing Blood Cells. Annual Review of Fluid Mechanics.

Oishi, M., Utsubo, K., Kinoshita, H., Fujii, T., Oshima, M., Oshima, M., 2012. Continuous and simulataneous measurement of the tank-treading motion of red blood cells and the surrounding flow using translational confocal micro-particle image velocimetry (micro-PIV) with sub-micron resolution. Meas. Sci. Technol. 23, 035301.

Olsen, M.G., Adrian, R.J., 2000. Out-of-focus effects on particle image visibility and correlation in microscopic particle image velocimetry. Exp Fluids 29, 166–174.

Ong, P.K., Jain, S., Kim, S., 2012. Spatio-temporal variations in cell-free layer formation near bifurcations of small arterioles. Microvascular Research 83, 118–125.

Poelma, C., Kloosterman, A., Hierck, B.P., Westerweel, J., 2012. Accurate Blood Flow Measurements: Are Artificial Tracers Necessary? PLoS ONE 7, e45247.

Pries, A.R., Ley, K., Claassen, M., Gaehtgens, P., 1989. Red cell distribution at microvascular bifurcations. Microvascular Research 38, 81–101.

Sherwood, J.M., Dusting, J., Kaliviotis, E., Balabani, S., 2012. The effect of red blood cell aggregation on velocity and cell-depleted layer characteristics of blood in a bifurcating microchannel. Biomicrofluidics 6, 24119.

Sherwood, J.M., Holmes, D., Kaliviotis, E., Balabani, S., 2014a. Spatial distributions of red blood cells significantly alter local haemodynamics. PLoS ONE Under review.

Sherwood, J.M., Kaliviotis, E., Dusting, J., Balabani, S., 2014b. Hematocrit, viscosity and velocity distributions of aggregating and non-aggregating blood in a bifurcating microchannel. Biomech Model Mechanobiol 13, 259–273.

Sugii, Y., Okuda, R., Okamoto, K., Madarame, H., 2005. Velocity measurement of both red blood cells and plasma of in vitro blood flow using high-speed micro PIV technique. Meas. Sci. Technol. 16, 1126–1130.

Westerweel, J., Scarano, F., 2005. Universal outlier detection for PIV data. Exp Fluids 39, 1096–1100.